processes

MDPI

Article

Computational Study of MHD Nanofluid Flow Possessing Micro-Rotational Inertia over a Curved Surface with Variable Thermophysical Properties

Zahid Ahmed [1], Ali Al-Qahtani [2], Sohail Nadeem [1] and Salman Saleem [2,*]

[1] Department of Mathematics, Quaid-i-Azam University, 45320, Islamabad 44000, Pakistan; zahidahmed@math.qau.edu.pk (Z.A.); snqau@hotmail.com (S.N.)

[2] Department of Mathematics, College of Sciences, King Khalid University, Abha 61413, Saudi Arabia; algahtani@kku.edu.sa

* Correspondence: saakhtar@kku.edu.sa or salmansaleem_33@hotmail.com; Tel.: +96-655-297-6805

Received: 12 May 2019; Accepted: 17 June 2019; Published: 21 June 2019

Abstract: This work presents a numerical investigation of viscous nanofluid flow over a curved stretching surface. Single-walled carbon nanotubes were taken as a solid constituent of the nanofluids. Dynamic viscosity was assumed to be an inverse function of fluid temperature. The problem is modeled with the help of a generalized theory of Eringen Micropolar fluid in a curvilinear coordinates system. The governing systems of non-linear partial differential equations consist of mass flux equation, linear momentum equations, angular momentum equation, and energy equation. The transformed ordinary differential equations for linear and angular momentum along with energy were solved numerically with the help of the Keller box method. Numerical and graphical results were obtained to analyze the flow characteristic. It is perceived that by keeping the dynamic viscosity temperature dependent, the velocity of the fluid away from the surface rose in magnitude with the values of the magnetic parameter, while the couple stress coefficient decreased with rising values of the magnetic parameter.

Keywords: carbon nanotubes; nanofluids; curved surface; variable viscosity; MHD

1. Introduction

During the past few years, the theory of nanofluids has obtained lot of importance due to its advancements in technology. The idea of the nanofluid was first introduced by Choi in 1995 [1]. The objective was to handle the heat management system. These new types of fluids are prepared in laboratories by suspending solid nano-sized particles in base fluid. The resulting composition is now a material with improved effective properties such as conductivity and density [2–10]. Due to their adjustable physical and thermophysical properties, nanofluids are used in wide range of applications [11–17]. The pertinency of these newly developed fluids in outspread industrial implications lure scientists to study nanofluids. Mention may be made some recent work of Raju et al. [18] in which they investigated the thermodynamics and mass convection of nanofluid with a radiated slender body. Sheikholeslami et al. [19] presented a study of nanofluid, where they also discussed the heat loss and transfer phenomena inside a pipe equipped with turbulators. Carbon nano tubes are amongst the nanoparticles that are commonly used due to their unique heat transfer abilities. They are sheets of graphite rolled in cylindrical shapes. They have an established capability of penetrating into cell membrane and support molecular cargo in loading and releasing medicines to the targeted area [20]. Nadeem et al. [21] studied the flow of heat and mass of carbon nanotube based nanofluids. In this study they have differentiated the effects of single walled and multi-walled carbon

nanotubes on the heat flow phenomena. In addition to above works, many other researchers have made important contributions to the field of nanofluids [22–31].

The theory of viscous fluid plays an important role in real life due to its tremendous applications in science and technology. For viscous fluids, scientists generally consider the case of constant viscosity because of simplicity, but in certain situations and with a more practical point of view, the viscosity of the fluid can be variable. There are three possibilities for variable viscosity. For liquids, viscosity can depend on space variables or temperature, whereas in solids or highly non-Newtonian fluids viscosity can be a function of pressure, in the cases of gases the viscosity may exhibit variations with density. For liquids the most feasible scenario is to consider the viscosity as a function of temperature. The variations in fluid temperature due to the heat transfer from the boundaries, heat produced by the inner friction of the nanofluid phases or other sources can disturb the fluid dynamic viscosity. The viscosity thus is no longer expected to be constant. The phenomenon can be observed in number of materials. For example: In water and coal slurries the viscosity varies with temperature variations. Viscosity of these fluids normally is inversely related to the temperature. A rise in temperature therefore may fasten the mass transport phenomena. To study the flow and thermodynamics of the fluid, it is therefore unavoidable to consider the temperature dependence of the dynamic viscosity. There are few useful studies which deal with viscosity being considered as a function of temperature [32–36].

The flow of a viscous fluid can usually be studied with the help of Navier Stokes equations. However, Navier Stokes equations can only take into consideration the motion of the fluid at macro level, while it cannot disclose the effects on fluid flow due to their micro-structure. On the other hand, the micro-polar fluid theory proposed by Eringen [37,38] can be incorporated into study spin or micro-rotational motion, and effects of these intrinsic motion on the flow of fluids across any channel. This theory is there for a good generalization of the Navier Stokes model. In addition to the forces that was assumed in the classical Navier Stokes model, Eringen took into account the several stresses that are responsible for the rotational inertia that develops in the fluid body. The stress tensors are composed of both a symmetric and an asymmetric part. For simplicity in the case of viscous fluid flow, only the symmetric part is taken. Since the phenomenon is very realistic, scientists consider it in their research, though it is still quite difficult to justify experimentally. Mention may be made of some important recent work by Ghadikolaei et al. [39], which shows the effects of magnetism and porosity on micropolar dusty fluids with metallic nano-particles. Nadeem et al. [40] presented a study that reveals the impact of magnetism and slip effects on micropolar hybrid nanofluid flow through a circular cylinder. Many other important work may be mentioned as well [41–43]. Also, applications of curvilinear surfaces involve the importance of pressure variations and its applications in curving jaws in producing machines. Besides that, curved surfaces are useful to tackle the deficiencies faced in any medical apparatus used for propelling fluids out of the containers. An example of this is a fluid dispensing apparatus with a prestressed bladder.

The principal goal of this work was to investigate the effects of temperature dependent viscosities on nanofluid flow while considering rotational inertia over a curvilinear surface. The boundary layer approximation is executed on linear and angular momentum equations coupled with an energy equation. The subsequent highly nonlinear ordinary differential equations are unraveled numerically with the help of a finite difference scheme known as the Keller box method. A detailed explanation of the mathematical procedure that has been followed is also used as an indication in the study. A reasonable comparison is also given for the simplest case.

2. Problem Considerations

The boundary layer as an incompressible and steady two-dimensional flow of a nanofluid over a curved stretching surface of radius R was considered. A single-walled carbon nanotube (SWCNT) was considered as a solid constituent of the nanofluid. $U_w(s)$ is the stretching velocity along the s-direction while $V_w(r)$ represent the mass flux through the porous surface. B is the applied externa magnetic field while the induced magnetic field is considered to be negligible. It was assumed that two different

phases of nanofluid (solid and liquid) lead to rotational inertia in the fluid body. Micropolar fluid model is therefore implemented to study the intrinsic motions such as micro-rotation and spin motion. The effective dynamic viscosity of the nanofluid is taken as an inverse function of temperature. Figure 1 depicts the flow geometry.

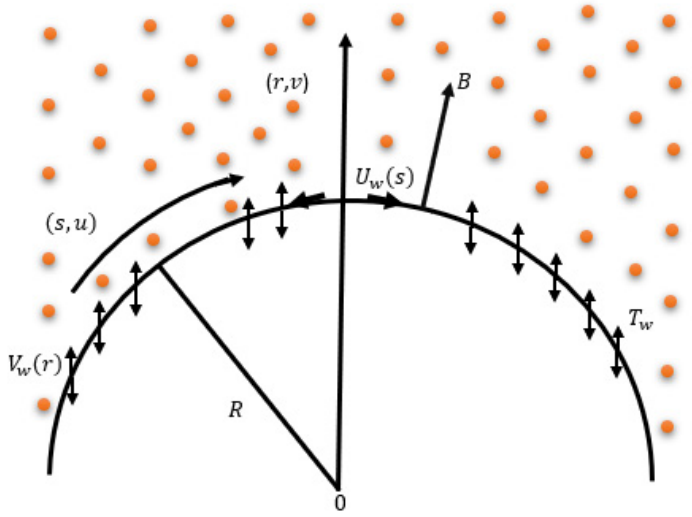

Figure 1. Functional diagram.

The governing equations in curvilinear coordinates can be written as.

$$\frac{\partial}{\partial r}[(r+R)v] + R\frac{\partial u}{\partial s} = 0 \tag{1}$$

$$\begin{aligned}\rho_{nf}\Big(v\tfrac{\partial v}{\partial r} + u\Big(\tfrac{R}{r+R}\Big)\tfrac{\partial v}{\partial s} - \tfrac{u^2}{r+R}\Big) \\ = -\tfrac{\partial p}{\partial r} + \tfrac{1}{(r+R)}\tfrac{\partial}{\partial r}\Big((r+R)\mu_{nf}\tfrac{\partial v}{\partial r}\Big) + \tfrac{R}{(r+R)}\tfrac{\partial}{\partial s}\Big(\mu_{nf}(\tfrac{\partial u}{\partial r} + \tfrac{R}{(r+R)}\tfrac{\partial v}{\partial s} - \tfrac{u}{r+R})\Big) \\ -\tfrac{1}{r+R}\mu_{nf}\Big(\tfrac{\partial u}{\partial r} + \tfrac{R}{(r+R)}\tfrac{\partial v}{\partial s} - \tfrac{u}{r+R}\Big)\end{aligned} \tag{2}$$

$$\rho_{nf}\left(v\frac{\partial u}{\partial r} + u\left(\frac{R}{r+R}\right)\frac{\partial u}{\partial s} + \frac{uv}{r+R}\right) = -\frac{R}{(r+R)}\frac{\partial p}{\partial s} + \frac{\partial}{\partial r}((\mu_{nf}+K_1)(\frac{\partial u}{\partial r} - \frac{u}{r+R})) - K_1\frac{\partial N}{\partial r} - \sigma B^2 u \tag{3}$$

$$\rho_{nf}j\left(v\frac{\partial N}{\partial r} + u\left(\frac{R}{r+R}\right)\frac{\partial N}{\partial s}\right) = -\frac{1}{(r+R)}\frac{\partial}{\partial r}\left(\gamma^*(r+R)\frac{\partial N}{\partial r}\right) - K_1(2N + \frac{\partial u}{\partial r} + \frac{u}{(r+R)}) \tag{4}$$

$$v\frac{\partial T}{\partial r} + \frac{R}{(r+R)}\frac{\partial T}{\partial s} = \alpha_{nf}\left(\frac{\partial^2 T}{\partial r^2} + \frac{1}{(r+R)}\frac{\partial T}{\partial r}\right) \tag{5}$$

The relevant boundary conditions are:

$$\left.\begin{array}{cccccc} u = \lambda U_w(s) & v = V_w(s,t) & T = T_w & at & r = 0 \\ u \to 0, & \frac{\partial u}{\partial r} \to 0 & T = T_\infty & at & r \to \infty \end{array}\right\} \tag{6}$$

u and v are the velocities in s and r directions, respectively. T is the fluid temperature, N is the angular velocity of the fluid element, p represents the pressure on the fluid, ρ_{nf}, $\left(\rho C_p\right)_{nf}$ *and* α_{nf} are the effective density, heat capacitance and thermal diffusibility of the nanofluid respectively. μ_{nf} is the effective dynamic viscosity of the nanofluid. K_1 represents the micro-rotation viscosity of the fluid where as $\gamma^* = j(\mu_{nf} + \frac{K_1}{2})$ is the spin gradient viscosity of the fluid. j is the micro-inertial density. The effective dynamic viscosity of the nanofluid can be written as $\mu_{nf} = \frac{\mu_f}{(1-\phi)^{2.5}}$, where μ_f is the coefficient of viscosity, which was taken as the inverse function of temperature. i.e., The expressions for effective

heat capacitance and density be $\rho_{nf} = (1-\phi)\rho_f + \phi\rho_s$ and $\left(\rho C_p\right)_{nf} = (1-\phi)\left(\rho C_p\right)_f + \phi\left(\rho C_p\right)_s$. We used Carbon nanotubes as solid particles, the effective thermal conductivity as given by the Xue model is $\frac{K_{nf}}{K_f} = \frac{1-\phi+2\phi\frac{K_s}{K_s-K_f}\ln\frac{K_s+K_f}{2K_f}}{1-\phi+2\phi\frac{K_f}{K_s-K_f}\ln\frac{K_s+K_f}{2K_f}}$. $U_w(s)$ is the stretching or shrinking velocity which was taken as $U_w(s) = as$, a is a dimensionless positive constant. λ is a dimensionless constant known as the stretching parameter. For stretching we only put > 0. We also took $V_w = -\sqrt{a\nu_\infty}S$, where S is a constant parameter that represent mass transfer through the surface. We considered the suction phenomena throughout the study. For suction we had $S > 0$.

Incorporating the boundary layer approximation for very large values of the Reynolds number, the governing nonlinear partial differential equations reduced to the form given below.

$$\rho_{nf}\left(\frac{u^2}{r+R}\right) = \frac{\partial p}{\partial r} \tag{7}$$

$$\rho_{nf}\left(v\frac{\partial u}{\partial r} + u\left(\frac{R}{r+R}\right)\frac{\partial u}{\partial s} + \frac{uv}{r+R}\right) = -\frac{R}{(r+R)}\frac{\partial p}{\partial s} + \left(\mu_{nf} + K_1\right)\frac{\partial^2 u}{\partial r^2} - \frac{\partial \mu_{nf}}{\partial r}\frac{u}{(r+R)} + \frac{\partial \mu_{nf}}{\partial r}\frac{\partial u}{\partial r} - K_1\frac{\partial N}{\partial r} - \sigma B^2 u \tag{8}$$

$$\rho_{nf} j\left(v\frac{\partial N}{\partial r} + u\left(\frac{R}{r+R}\right)\frac{\partial N}{\partial s}\right) = -\frac{1}{(r+R)}\frac{\partial}{\partial r}\left(\gamma^*(r+R)\frac{\partial N}{\partial r}\right) - K_1\left(2N + \frac{\partial u}{\partial r} + \frac{u}{(r+R)}\right)$$

$$v\frac{\partial T}{\partial r} + \frac{R}{(r+R)}\frac{\partial T}{\partial s} = \alpha_{nf}\left(\frac{\partial^2 T}{\partial r^2} + \frac{1}{(r+R)}\frac{\partial T}{\partial r}\right) \tag{9}$$

The boundary conditions now became:

$$\left.\begin{array}{cccccc} u = \lambda\, as & v = -\sqrt{a\nu_\infty}S & T = T_w & at & r = 0 \\ u \to 0 & \frac{\partial u}{\partial r} \to 0 & T = T_\infty & at & r \to \infty. \end{array}\right\} \tag{10}$$

Choosing suitable similarity transformations and introducing dimensionless functions f, θ and similarity variable η

$$\begin{array}{l} u = asf'(\eta),\ v = -\frac{R}{r+R}\sqrt{a\nu_\infty}f(\eta),\ \theta = \frac{T-T_\infty}{T_w-T_\infty} \\ \eta = \sqrt{\frac{a}{\nu_\infty}}r \quad p = \rho_{nf}a^2s^2P(\eta) \end{array} \tag{11}$$

Applying the above similarity transformations, the momentum and energy equations were transformed into the following system of non-linear Ordinary differential equations:

$$\frac{\partial P}{\partial \eta} = \frac{f'^2}{\eta+\kappa} \tag{12}$$

$$\frac{2\kappa}{(\eta+\kappa)}P(\eta) = \frac{1}{A_1}\left(\left(1+K(1-\phi)^{2.5}\right)\left(\frac{f'''}{\left(1-\frac{\theta}{\theta_r}\right)} + \frac{1}{(\eta+\kappa)}\frac{f''}{\left(1-\frac{\theta}{\theta_r}\right)} - \frac{1}{(\eta+\kappa)^2}\frac{f'}{\left(1-\frac{\theta}{\theta_r}\right)}\right) - \frac{1}{(\eta+\kappa)}\frac{f'\theta'}{\theta_r\left(1-\frac{\theta}{\theta_r}\right)^2} + \frac{f''\theta'}{\theta_r\left(1-\frac{\theta}{\theta_r}\right)^2} - M_1 f'\right) \tag{13}$$
$$+\frac{\kappa}{(\eta+\kappa)}\left(ff'' - f'^2 + \frac{1}{(\eta+\kappa)}ff'\right) - \frac{K(1-\phi)^{2.5}}{A_1}g'$$

$$\left(\frac{1}{\left(1-\frac{\theta}{\theta_r}\right)} + \frac{K(1-\phi)^{2.5}}{2}\right)\left(g'' + \frac{g'}{(\eta+\kappa)} + \frac{g'\theta'}{\theta_r\left(1-\frac{\theta}{\theta_r}\right)^2}\right)$$
$$- K(1-\phi)^{2.5}\left(2g + f'' + \frac{f'}{(\eta+\kappa)}\right) + A_1\frac{\kappa}{(\eta+\kappa)}(fg' - f'g) = 0 \tag{14}$$

$$\theta'' + \frac{1}{(\eta+\kappa)}\theta' + Pr\frac{\epsilon_2}{\epsilon_1}\frac{\kappa}{(\eta+\kappa)}f\theta' = 0 \tag{15}$$

where the differentiation is with respect to η and the symbols used are defined below:

$$A_1 = (1-\phi)^{2.5}\left[(1-\phi)+\phi\frac{\rho_s}{\rho_f}\right],\ \alpha_{nf} = \frac{K_{nf}}{(\rho C_p)_{nf}},\ Pr = \frac{\mu_f(\rho Cp)_f}{\rho_f K_f}$$

$$\epsilon_1 = \frac{1-\phi+2\phi\frac{K_s}{K_s-K_f}\ln\frac{K_s+K_f}{2K_f}}{1-\phi+2\phi\frac{K_f}{K_s-K_f}\ln\frac{K_s+K_f}{2K_f}},\ \epsilon_2 = (1-\phi)+\phi\frac{\left(\rho C_p\right)_s}{\left(\rho C_p\right)_f},\quad M_1 = (1-\phi)^{2.5}M^2$$

Using (11) into (12) we get

$$\begin{aligned}\left(1+K(1-\phi)^{2.5}\right)&\left(\frac{(\eta+\kappa)f^{iv}}{\left(1-\frac{\theta}{\theta_r}\right)}+\frac{2f'''}{\left(1-\frac{\theta}{\theta_r}\right)}-\frac{1}{(\eta+\kappa)}\frac{f''}{\left(1-\frac{\theta}{\theta_r}\right)}+\frac{1}{(\eta+\kappa)^2}\frac{f'}{\left(1-\frac{\theta}{\theta_r}\right)}\right)\\&+\frac{2(\eta+\kappa)f'''\theta'}{\theta_r\left(1-\frac{\theta}{\theta_r}\right)^2}+\frac{f''\theta'}{\theta_r\left(1-\frac{\theta}{\theta_r}\right)^2}-\frac{f'\theta''}{\theta_r\left(1-\frac{\theta}{\theta_r}\right)^2}-\frac{2f'\theta'}{\theta_r{}^2\left(1-\frac{\theta}{\theta_r}\right)^3}\\&+\frac{(\eta+\kappa)f''\theta''}{\theta_r\left(1-\frac{\theta}{\theta_r}\right)^2}+\frac{2(\eta+\kappa)f''\theta'}{\theta_r{}^2\left(1-\frac{\theta}{\theta_r}\right)^3}-\frac{1}{(\eta+\kappa)}\frac{f'\theta'}{\theta_r\left(1-\frac{\theta}{\theta_r}\right)^2}\\&-M_1(f'+(\eta+\kappa)f'')+\kappa A_1(ff'''-f'f'')\\&+\frac{\kappa}{(\eta+\kappa)}A_1\left(ff''-f'^2-\frac{1}{(\eta+\kappa)}ff'\right)\\&-K(1-\phi)^{2.5}\left(\frac{(\eta+\kappa)g''}{\left(1-\frac{\theta}{\theta_r}\right)}+\frac{g'}{\left(1-\frac{\theta}{\theta_r}\right)}\right)=0\end{aligned}\tag{16}$$

$$\begin{aligned}\left(\frac{1}{\left(1-\frac{\theta}{\theta_r}\right)}+\frac{K(1-\phi)^{2.5}}{2}\right)&\left(g''+\frac{g'}{(\eta+\kappa)}+\frac{g'\theta'}{\theta_r\left(1-\frac{\theta}{\theta_r}\right)^2}\right)\\&-K(1-\phi)^{2.5}\left(2g+f''+\frac{f'}{(\eta+\kappa)}\right)+A_1\frac{\kappa}{(\eta+\kappa)}(fg'-f'g)=0\end{aligned}\tag{17}$$

$$\theta''+\frac{1}{(\eta+\kappa)}\theta'+Pr\frac{\epsilon_2}{\epsilon_1}\frac{\kappa}{(\eta+\kappa)}f\theta'=0\tag{18}$$

Now the boundary conditions in dimensionless form became:

$$f=S\quad f'=\lambda\quad \theta=1\ at\ \eta=0$$

$$f'\to 0\ f''\to 0,\ \theta\to 0\ as\ \eta\to\infty$$

We are also interested in finding the skin friction coefficient (C_{fr}), Couple stress (C_{mr}) and Nusselt number (Nu) near the boundaries, which can be written as $C_{fr}{Re_s}^{1/2} = \frac{1}{(1-\phi)^{2.5}\left(1-\frac{1}{\theta_r}\right)}(1+K)\left(f''(0)-\frac{1}{\kappa}\right)$, $C_{mr}{Re_s}^{1/2} = \frac{1}{(1-\phi)^{2.5}\left(1-\frac{1}{\theta_r}\right)}\left(1+\frac{K}{2}\right)\left(g'(0)-N_0\frac{f''(0)}{\kappa}\right)$ and $Nu{Re_s}^{1/2} = -\epsilon_1\theta'(0)$, where $Re_s = \frac{as^2}{\nu_{f\infty}}$ is the local Reynolds number.

Solution Procedure

The Eringin theory of micropolar fluid was used to model the assumed problem. The governing system of equations were a set of five non-linear partial differential equations in curvilinear coordinates. Boundary layer approximation is incorporate on the system of equations to avoid the terms of negligible effects. Suitable similarity transformations were implemented on the system. The reduced system of similar equations was now set of non-linear ordinary differential equations. The entity of temperature dependent viscosity molded the momentum equations to be highly non-linear. A powerful finite difference scheme "Keller box" was used to solve the governing system of simultaneous non-linear ordinary differential equations. This technique consists of four separate procedures. The very first step is to convert the governing equations into a set of first order differential equations. In the second

phase these equations are discretized using a central difference scheme, followed by linearization with Newton's linearization. The very last step is to write the linearized set of algebraic equations into block tri-diagonal form and solve by matrix algebra. Numerical and graphical results are obtained by programming this very last step into MATLAB. Table 1 is shows thermophysical properties of base and nanofluids. For the purpose of solution authentication, a simplest case of the problem was compared with a previous published result. Data appear to be in very good agreement with the published results, as can be seen in Table 2. Tecplot 360 was also utilized to plot streamlines and isotherms. $\eta_\infty = 16$ was set as the edge of the boundary layer. A very fine Step size of $\triangle\eta = 0.005$ was taken for the calculations. Error tolerance was set at 10^{-6}.

Table 1. Thermo-physical properties of the base fluid and nanoparticles.

Thermo-Physical Properties	Pure-Water	SWCNT	MWCNT
$C_p(J/kgK)$	4179	425	796
$\rho\left(kg/m^3\right)$	997.1	2600	1600
$k\,(W/mK)$	0.613	6600	3000

Table 2. Comparison of $-C_{fr}{Re_s}^{1/2}$ with different values of curvature parameter. $\lambda = 1$, $M = 0$, $\phi = 0.0$, $\theta_r \to \infty$.

κ	Roşca et al. [44]	Present Results
5	1.15076	1.20000
10	1.07172	1.10000
20	1.03501	1.05001
30	1.02315	1.03331
40	1.01729	1.02503
50	1.01380	1.02001
100	1.00687	1.01002
200	1.00342	1.00504
1000	1.00068	1.00100
∞	1.00000	1.00000

3. Results and Discussion

Equations (16)–(18) are governing non-linear ordinary differential equations. The above system of simultaneous equations was solved numerically with a powerful finite difference scheme with the help of MATLAB software (R2013 A, MathWorks, Natick, MA, USA). Numerical results obtained were then represented graphically with the help of MATLAB and Tecplot (2015 R1, tecplot, Bellevue, WA, USA) graphic utility. Figures 2 and 3 shows streamline patterns and pressure variation, respectively. A comparison study was also performed to authenticate our solution. Table 2 represents both the present study and a published result by Rosca et al. Both results have a very good order of agreement.

Figures 4–6 are isotherm plots executed with different physical parameters. It can be concluded from the results that temperature distribution within the fluid rises with an increase in the curvature parameter, as well as with the solid fractions of single walled carbon nanotubes. Suction on the other hand lowered the temperatures of the fluid, as can be seen in Figure 6a–c. Velocity profile along s-direction are represented in Figure 7a–c with different physical parameters. It can be seen that the flow was opposed by curvature parameter as well as suction parameter, whereas flow of the fluid rose for increasing values of the magnetic parameter. Figure 8a–d depicts variations in the skin friction coefficient near the boundaries, where Figure 9a–e are couple stress plots near the curved surface. Graphical results show that skin friction as well as a couple stress parameter decreased for the micropolar parameter, variable viscosity parameter and suction parameter. Besides that, a decrease in couple stress with rising values of magnetic parameter can be seen from Figure 9c. For an ascending magnitude of curvature parameter, it can be seen that the skin friction profile increased, whereas couple stress decreased. Behavior of the temperature gradient near the surface can be understood with the help

of the Nusselt number and solid fraction graphs. Figure 10a gives a comparison between two different types of carbon nanotubes with different physical and thermal properties for effective heat transfer enhancement. Both single-walled carbon nanotubes (SWCNT) and multi-walled carbon nanotubes (MWCNT) exhibited similar behavior for changing values of Prandtl number. i.e., In both cases the Nusselt number increased in magnitude, however SWCNT as a solid constituent always enhanced the heat transfer capability of the fluid, as can be seen in Figure 10a–c, which show a decrease in Nusselt number with rising values of curvature and variable viscosity parameters, whereas Figure 10d validates an increment in the temperature gradient near the wall with increasing values of the suction parameter.

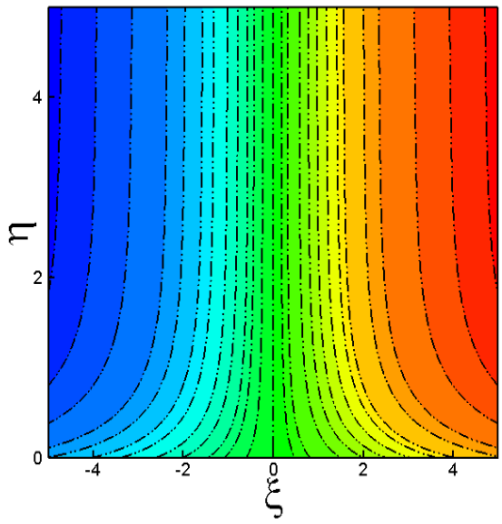

Figure 2. Streamlines pattern.

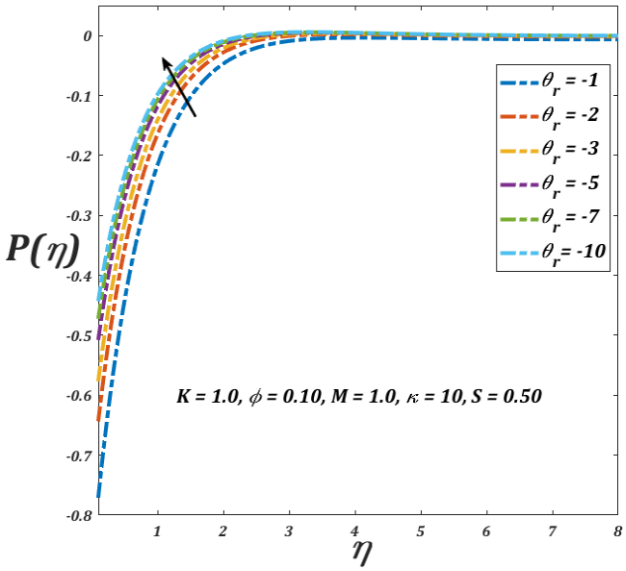

Figure 3. Pressure variation with Variable viscosity parameter.

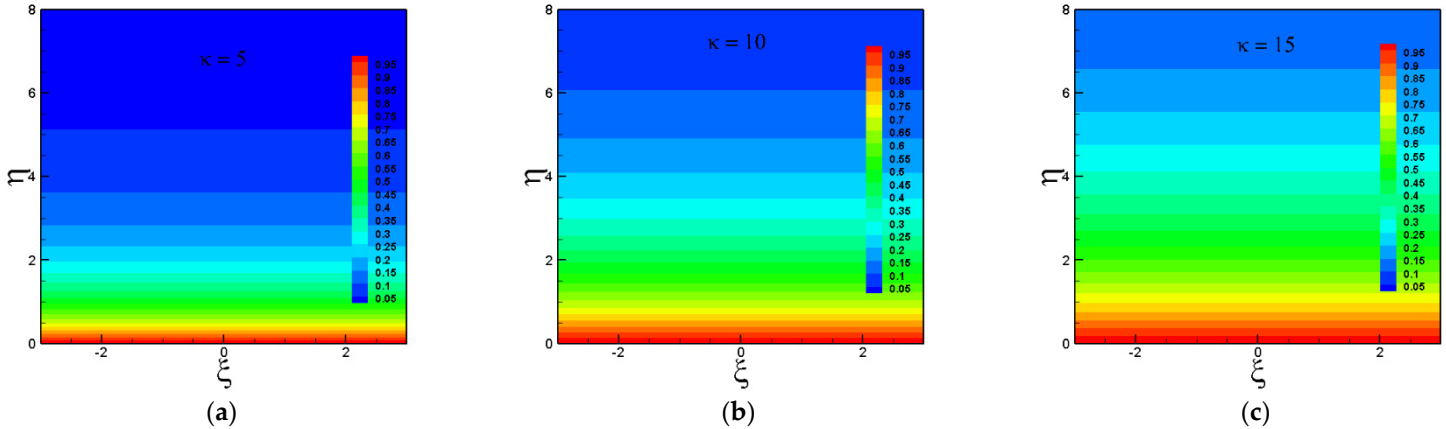

Figure 4. (**a**). Isotherm with $\kappa = 5$. (**b**). Isotherm with $\kappa = 10$. (**c**). Isotherm with $\kappa = 15$.

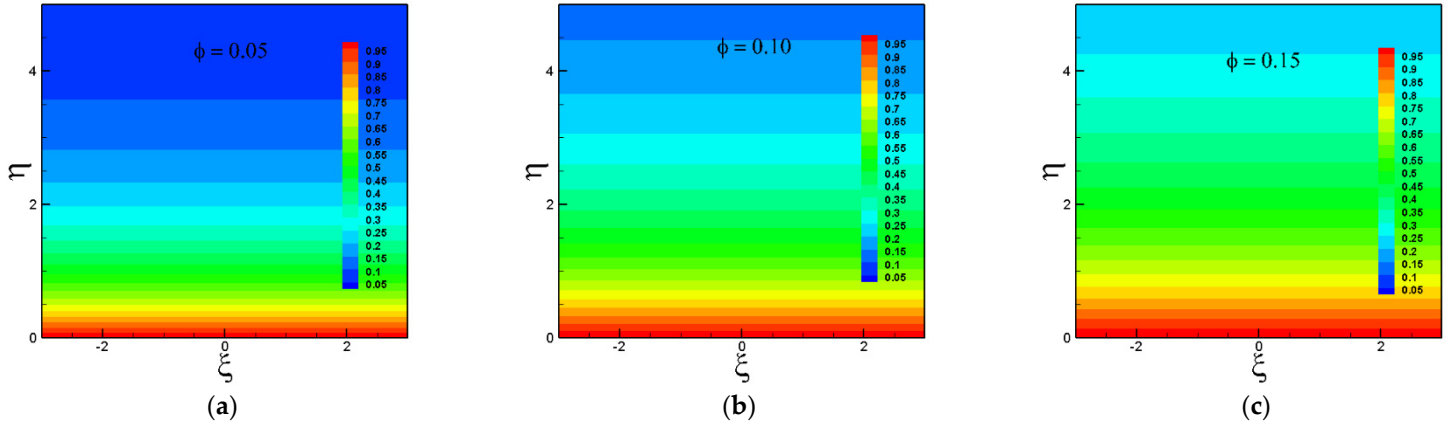

Figure 5. (**a**). Isotherm with $\phi = 0.05$. (**b**). Isotherm with $\phi = 0.10$. (**c**). Isotherm with $\phi = 0.15$.

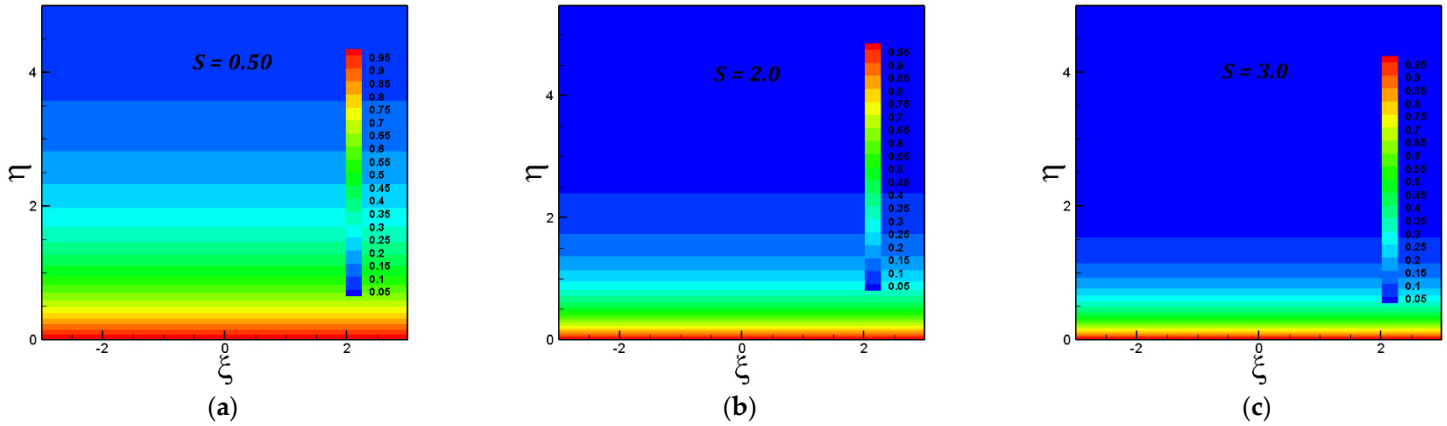

Figure 6. (**a**). Isotherm with $S = 0.50$. (**b**). Isotherm with $S = 2.0$. (**c**). Isotherm with $S = 3.0$.

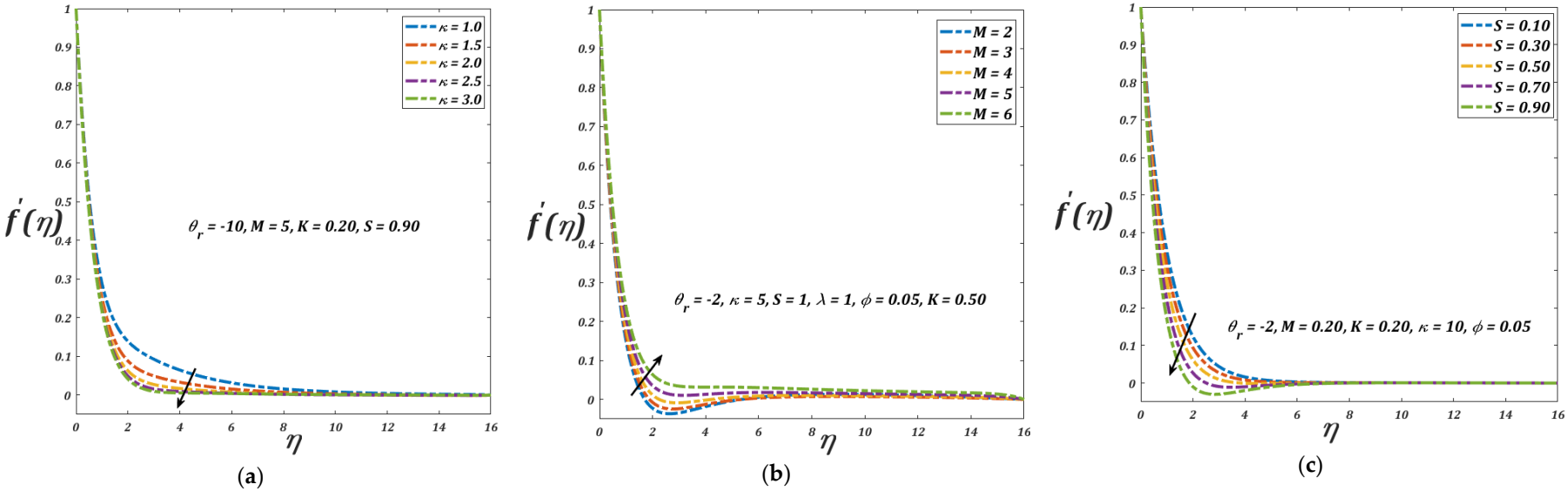

Figure 7. (**a**). Variation in velocity with Curvature parameter. (**b**). Variation in velocity with Magnetic parameter. (**c**). Variation in velocity with Porosity parameter.

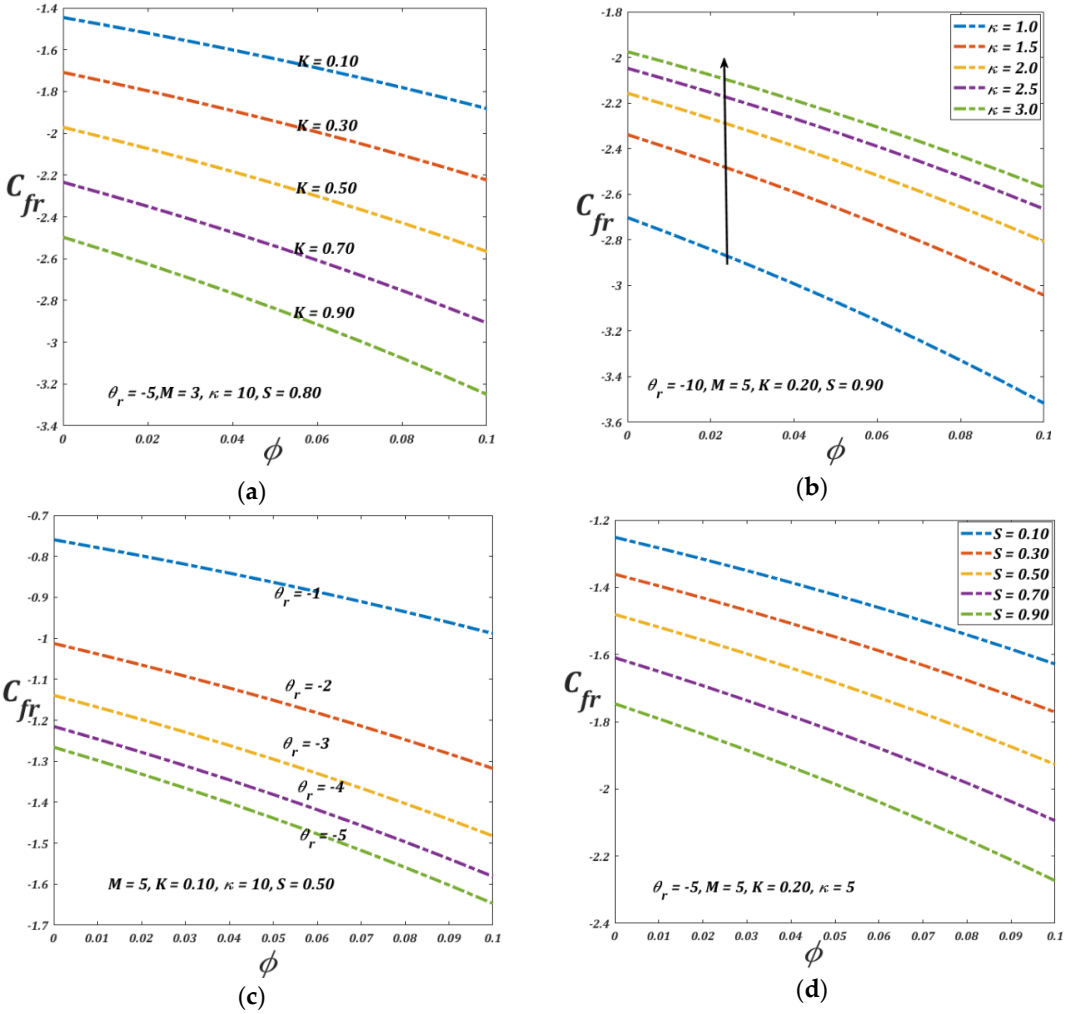

Figure 8. (**a**) Skin friction Coefficient with Micropolar parameter. (**b**). Skin friction coeffiecient with curvature parameter. (**c**). Skin friction coefficient with variable viscosity parameter. (**d**). Skin friction with porosity parameter.

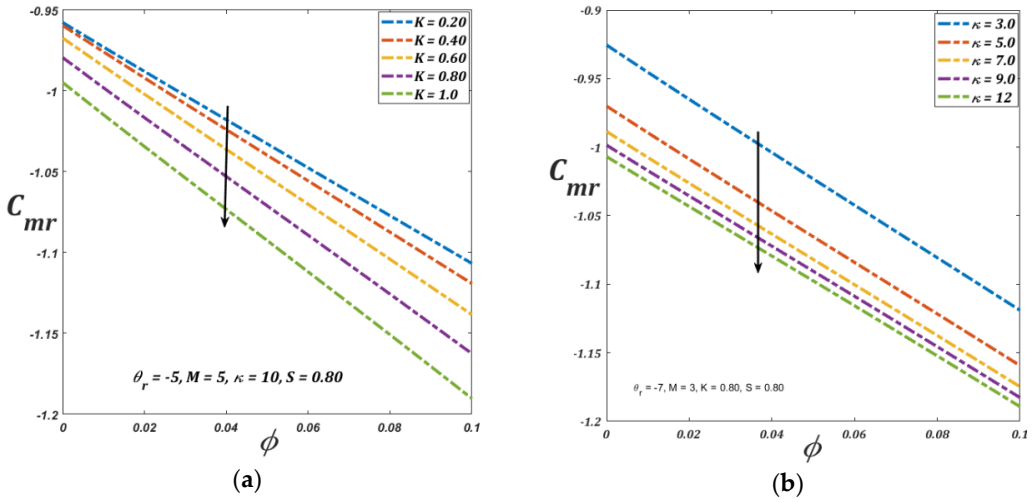

Figure 9. *Cont.*

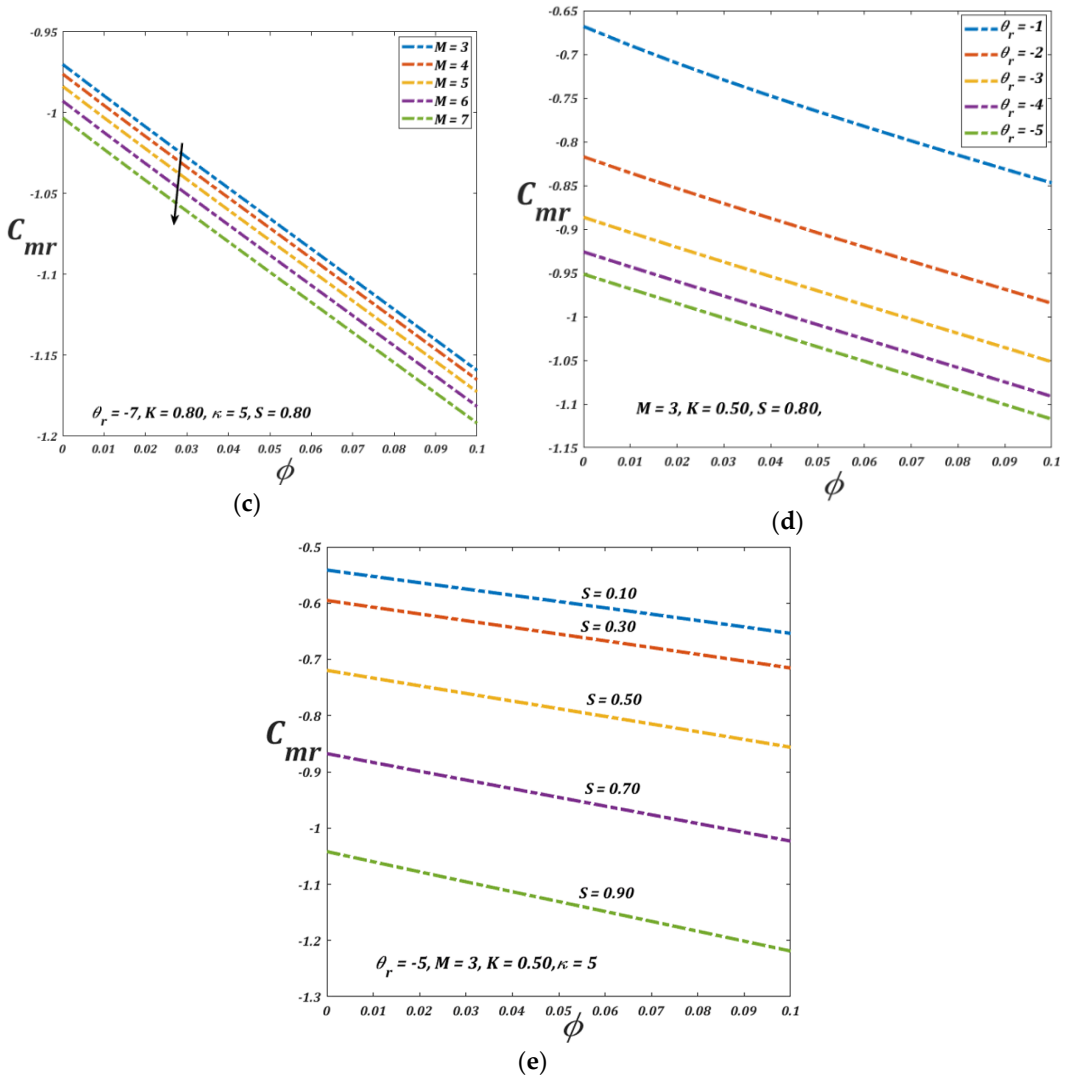

Figure 9. (**a**). Skin friction with micropolar parameter. (**b**). Couple stress coefficient with curvature parameter. (**c**). Couple stress coefficient with magnetic parameter. (**d**). Couple stress with variable viscosity parameter. (**e**). Couple stress with porosity parameter.

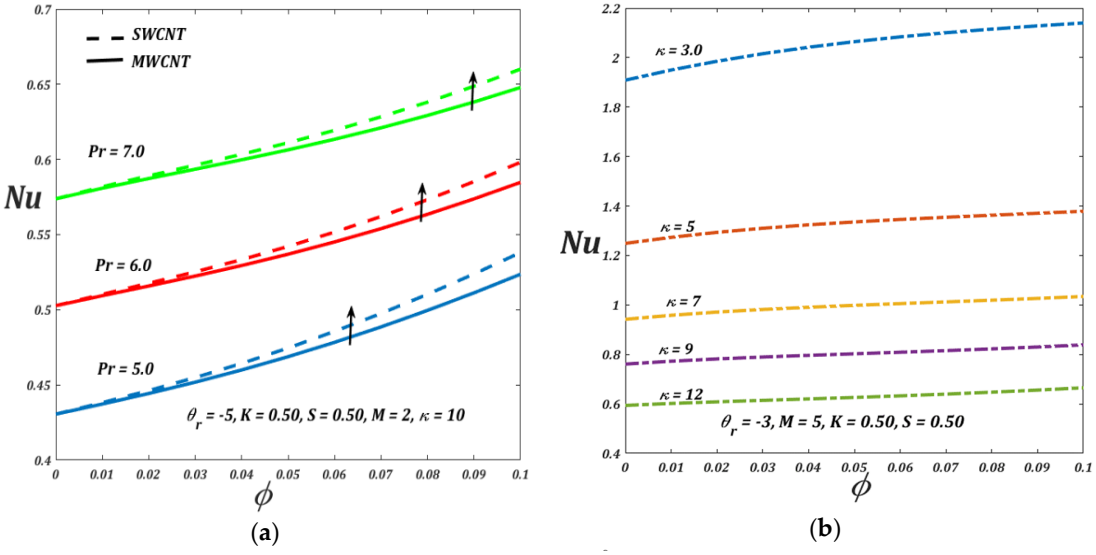

Figure 10. *Cont.*

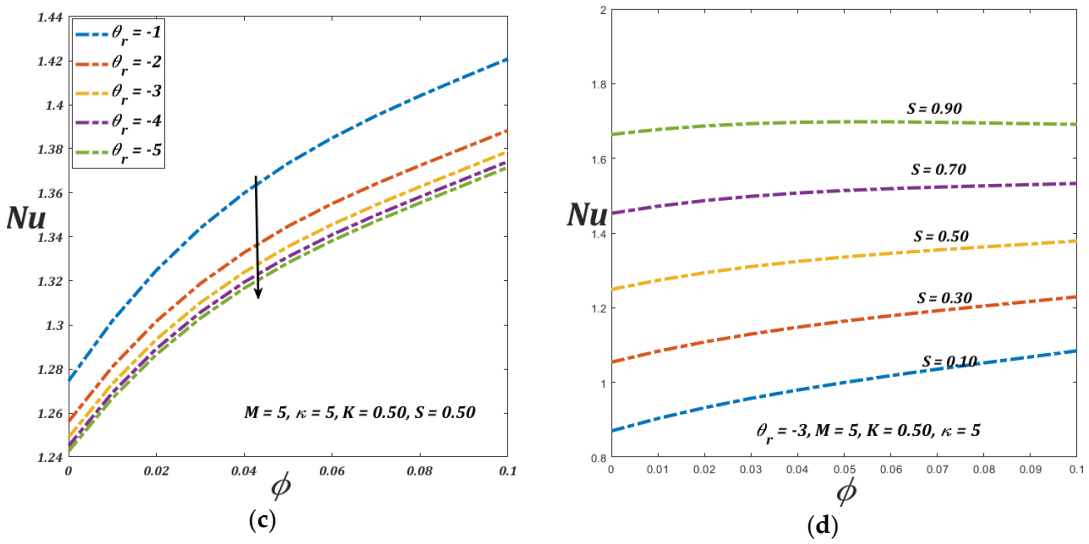

Figure 10. (**a**). Nusselt number with Pr for SWCNT and MWCNT. (**b**). Nusselt number with curvature parameter. (**c**). Nusselt number with variable viscosity parameter. (**d**). Nusselt number with suction parameter.

4. Conclusions

These reevaluation efforts were commendable enough to classify the enhancement in heat transfer and thermal conductivity of micropolar fluid with nanoparticle conductive properties. Dynamic viscosity is supposed to be an inverse function of fluid temperature. It has been concluded that with a variable dynamic viscosity, the velocity distribution of the fluid increases with magnetic parameter, whereas an increase in the magnitude of variable viscosity parameter resists the fluid flow. Within the proposed circumstances of temperature dependent viscosities, the magnitude of skin friction drops with rising values of micropolar parameter, while it rises with the increasing magnitude of the curvature parameter. Also, results show that the heat transfer coefficient is enhanced when using single-walled carbon nanotubes as compared to when using multi-walled carbon nanotubes. The employed method was compared with already available results for the authentication of our technique. Lastly, such physical problems of curved surfaces are useful to tackle the deficiencies faced in medical devices used for propelling fluids out of containers.

Author Contributions: Conceptualization, Z.A. and S.S.; Methodology, Z.A.; Software, Z.A.; Validation, Z.A.; Formal Analysis, Z.A.; Investigation, S.S.; Resources, S.N.; Data Curation, S.N.; Writing-Original Draft Preparation, Z.A.; Writing-Review & Editing, S.N. and A.A.-Q.; Visualization, S.S.; Supervision, S.N.; Project Administration, S.S.; Funding Acquisition, A.A.-Q.

Funding: The authors extend their appreciation to the Deanship of Scientific Research at King Khalid University for funding this work through research groups program under Grant No. R.G.P.2/51/40.

Acknowledgments: The authors extend their appreciation to the Deanship of Scientific Research at King Khalid University for funding this work through research groups program under Grant No. R.G.P.2/51/40.

Conflicts of Interest: The authors declare no conflict of interest.

Nomenclature

u, v	Velocities along s and r axis respectively.	T_w, T_∞	Temperature at the boundary and at far away respectively
ρ_{nf}, μ_{nf}	Effective density and dynamic viscosity of nanofluid	f, θ	Dimensionless velocity and temperature respectively
p	Fluid pressure	θ_r	Variable viscosity parameter

$B(t)$, σ	Magnetic field and electric charge density respectively	K_{nf}, α_{nf}	Thermal conductivity and diffusivity of nanofluid
σ_e	Stefan Boltzmann constant	ϕ	Volume fraction of CNT
κ	Curvature parameter	β_R	Mean absorption constant
K	Micropolar parameter		
T	Fluid temperature	M, Pr	Magnetic parameter and Prandtl number respectively

References

1. Choi, S.U.S.; Eastman, J.A. *Enhancing Thermal Conductivity of Fluids with Nanoparticles*; Argonne National Lab.: Lemont, IL, USA, 1995.
2. Dombek, G.; Nadolny, Z.; Marcinkowska, A. Effects of nanoparticles materials on heat transfer in electro-insulating liquids. *Appl. Sci.* **2018**, *8*, 2538. [CrossRef]
3. Nadolny, Z.; Dombek, G. Electro-insulating nanofluids based on synthetic ester and TiO2 or C60 nanoparticles in power transformer. *Energies* **2018**, *11*, 1953. [CrossRef]
4. Xue, Q.-Z. Model for effective thermal conductivity of nanofluids. *Phys. Lett. A* **2003**, *307*, 313–317. [CrossRef]
5. Saleem, S.; Nadeem, S.; Rashidi, M.M.; Raju, C.S.K. An optimal analysis of radiated nanomaterial flow with viscous dissipation and heat source. *Microsyst. Technol.* **2019**, *25*, 683–689. [CrossRef]
6. Sadiq, M.A.; Khan, A.U.; Saleem, S.; Nadeem, S. Numerical simulation of oscillatory oblique stagnation point flow of a magneto micropolar nanofluid. *RSC Adv.* **2019**, *9*, 4751–4764. [CrossRef]
7. Ullah, A.; Shah, Z.; Kumam, P.; Ayaz, M.; Islam, S.; Jameel, M. Viscoelastic MHD Nanofluid Thin Film Flow over an Unsteady Vertical Stretching Sheet with Entropy Generation. *Processes* **2019**, *7*, 262. [CrossRef]
8. Li, Z.; Saleem, S.; Shafee, A.; Chamkha, A.J.; Du, S. Analytical investigation of nanoparticle migration in a duct considering thermal radiation. *J. Therm. Anal. Calorim.* **2019**, *135*, 1629–1641. [CrossRef]
9. Li, Z.; Sheikholeslami, M.; Shafee, A.; Saleem, S.; Chamkha, A.J. Effect of dispersing nanoparticles on solidification process in existence of Lorenz forces in a permeable media. *J. Mol. Liq.* **2018**, *266*, 181–193. [CrossRef]
10. Saleem, S.; Rafiq, H.; Al-Qahtani, A.; El-Aziz, M.A.; Malik, M.Y.; Animasaun, I.L. Magneto Jeffrey Nanofluid Bioconvection over a Rotating Vertical Cone due to Gyrotactic Microorganism. *Math. Probl. Eng.* **2019**, *2019*. [CrossRef]
11. Sidik, N.A.C.; Yazid, M.N.A.W.M.; Mamat, R. A review on the application of nanofluids in vehicle engine cooling system. *Int. Commun. Heat Mass Transf.* **2015**, *68*, 85–90. [CrossRef]
12. Bianco, A.; Kostarelos, K.; Prato, M. Applications of carbon nanotubes in drug delivery. *Curr. Opin. Chem. Biol.* **2005**, *9*, 674–679. [CrossRef] [PubMed]
13. Huminic, G.; Huminic, A. Application of nanofluids in heat exchangers: A review. *Renew. Sustain. Energy Rev.* **2012**, *16*, 5625–5638. [CrossRef]
14. Keshmiri, K.; Mozaffari, S.; Tchoukov, P.; Huang, H.; Nazemifard, N. Using microfluidic device to study rheological properties of heavy oil. *arXiv* **2016**, arXiv:1611.10163.
15. Daivis, P.; Todd, B. Challenges in Nanofluidics—Beyond Navier–Stokes at the Molecular Scale. *Processes* **2018**, *6*, 144. [CrossRef]
16. Sooppy, N.S.K.; Gul, T.; Khan, W.; Tahir, M.; Bilal, R.; Khan, I. Unsteady Nano-Liquid Spray with Thermal Radiation Comprising CNTs. *Processes* **2019**, *7*, 181.
17. Nadeem, S.; Ahmed, Z.; Saleem, S. Carbon nanotubes effects in magneto nanofluid flow over a curved stretching surface with variable viscosity. *Microsyst. Technol.* **2018**, 1–8. [CrossRef]
18. Raju, C.S.K.; Saleem, S.; Mamatha, S.U.; Hussain, I. Heat and mass transport phenomena of radiated slender body of three revolutions with saturated porous: Buongiorno's model. *Int. J. Therm. Sci.* **2018**, *132*, 309–315. [CrossRef]
19. Sheikholeslami, M.; Jafaryar, M.; Saleem, S.; Li, Z.; Shafee, A.; Jiang, Y. Nanofluid heat transfer augmentation and exergy loss inside a pipe equipped with innovative turbulators. *Int. J. Heat Mass Transf.* **2018**, *126*, 156–163. [CrossRef]
20. Li, R.; Wu, R.; Zhao, L.; Hu, Z.; Guo, S.; Pan, X.; Zou, H. Folate and iron difunctionalized multiwall carbon nanotubes as dual-targeted drug nanocarrier to cancer cells. *Carbon* **2011**, *49*, 1797–1805. [CrossRef]

21. Nadeem, S.; Khan, A.U.; Hussain, S.T. Model based study of SWCNT and MWCNT thermal conductivities effect on the heat transfer due to the oscillating wall conditions. *Int. J. Hydrog. Energy* **2017**, *42*, 28945–28957. [CrossRef]
22. Sheikholeslami, M.; Zeeshan, A. Numerical simulation of Fe3O4-water nanofluid flow in a non-Darcy porous media. *Int. J. Numer. Methods Heat Fluid Flow* **2018**, *28*, 641–660. [CrossRef]
23. Hayat, T.; Nadeem, S.; Khan, A.U. Rotating flow of Ag-CuO/H 2 O hybrid nanofluid with radiation and partial slip boundary effects. *Eur. Phys. J. E* **2018**, *41*, 75. [CrossRef]
24. Kumar, R.; Sood, S.; Shehzad, S.A.; Sheikholeslami, M. Radiative heat transfer study for flow of non-Newtonian nanofluid past a Riga plate with variable thickness. *J. Mol. Liq.* **2017**, *248*, 143–152. [CrossRef]
25. Akbar, N.S.; Khan, Z.H. Variable fluid properties analysis with water based CNT nanofluid over a sensor sheet: Numerical solution. *J. Mol. Liq.* **2017**, *232*, 471–477. [CrossRef]
26. Subhani, M.; Nadeem, S. Numerical analysis of micropolar hybrid nanofluid. *Appl. Nanosci.* **2018**, *9*, 447–459. [CrossRef]
27. Qureshi, M.Z.A.; Rubbab, Q.; Irshad, S.; Ahmad, S.; Aqeel, M. Heat and mass transfer analysis of mhd nanofluid flow with radiative heat effects in the presence of spherical au-metallic nanoparticles. *Nanoscale Res. Lett.* **2016**, *11*, 472. [CrossRef]
28. Mozaffari, A.; Sharifi-Mood, N.; Koplik, J.; Maldarelli, C. Self-diffusiophoretic colloidal propulsion near a solid boundary. *Phys. Fluids* **2016**, *28*, 53107. [CrossRef]
29. Mozaffari, S.; Tchoukov, P.; Mozaffari, A.; Atias, J.; Czarnecki, J.; Nazemifard, N. Capillary driven flow in nanochannels–Application to heavy oil rheology studies. *Colloids Surf. A Physicochem. Eng. Asp.* **2017**, *513*, 178–187. [CrossRef]
30. Mozaffari, S.; Tchoukov, P.; Atias, J.; Czarnecki, J.; Nazemifard, N. Effect of asphaltene aggregation on rheological properties of diluted athabasca bitumen. *Energy Fuels* **2015**, *29*, 5595–5599. [CrossRef]
31. Mozaffari, S.; Li, W.; Thompson, C.; Ivanov, S.; Karim, A. Kinetic Treatment of the Metal-Ligand Binding for Predictive Synthesis of Colloidal Nanoparticles. In Proceedings of the Abstracts of Papers of the American Chemical Society, Boston, MA, USA, 19–23 August 2018; American Chemical Society: Washington, DC, USA, 2018; Volume 255.
32. Ellahi, R. The effects of MHD and temperature dependent viscosity on the flow of non-Newtonian nanofluid in a pipe: Analytical solutions. *Appl. Math. Model.* **2013**, *37*, 1451–1467. [CrossRef]
33. Nadeem, S.; Ahmed, Z.; Saleem, S. The Effect of Variable Viscosities on Micropolar Flow of Two Nanofluids. *Z. Naturforschung Sect. A J. Phys. Sci.* **2016**, *71*. [CrossRef]
34. Shahzadi, I.; Nadeem, S.; Rabiei, F. Simultaneous effects of single wall carbon nanotube and effective variable viscosity for peristaltic flow through annulus having permeable walls. *Results Phys.* **2017**, *7*, 667–676. [CrossRef]
35. Akbar, N.S.; Tripathi, D.; Khan, Z.H. Numerical Simulation of Nanoparticles with Variable Viscosity over a Stretching Sheet. In *Numerical Simulations in Engineering and Science*; IntechOpen: London, UK, 2018.
36. Xun, S.; Zhao, J.; Zheng, L.; Zhang, X. Bioconvection in rotating system immersed in nanofluid with temperature dependent viscosity and thermal conductivity. *Int. J. Heat Mass Transf.* **2017**, *111*, 1001–1006. [CrossRef]
37. Eringen, A.C. Simple microfluids. *Int. J. Eng. Sci.* **1964**, *2*, 205–217. [CrossRef]
38. Eringen, A.C. Theory of thermomicrofluids. *J. Math. Anal. Appl.* **1972**, *38*, 480–496. [CrossRef]
39. Ghadikolaei, S.S.; Hosseinzadeh, K.; Hatami, M.; Ganji, D.D. MHD boundary layer analysis for micropolar dusty fluid containing Hybrid nanoparticles (Cu-Al2O3) over a porous medium. *J. Mol. Liq.* **2018**, *268*, 813–823. [CrossRef]
40. Nadeem, S.; Abbas, N. On both MHD and slip effect in Micropolar Hybrid nanofluid past a circular cylinder under stagnation point region. *Can. J. Phys.* **2018**, *97*, 392–399. [CrossRef]
41. Subhani, M.; Nadeem, S. Numerical analysis of 3D micropolar nanofluid flow induced by an exponentially stretching surface embedded in a porous medium. *Eur. Phys. J. Plus* **2017**, *132*, 441. [CrossRef]
42. Akbar, N.S.; Tripathi, D.; Khan, Z.H.; Bég, O.A. Mathematical modelling of pressure-driven micropolar biological flow due to metachronal wave propulsion of beating cilia. *Math. Biosci.* **2018**, *301*, 121–128. [CrossRef]

43. Ahmed, Z.; Nadeem, S. Flow of a Micropolar CNT based nanofluid across a squeezing channel. *Phys. Scr.* **2019**. [CrossRef]
44. Roşca, N.C.; Pop, I. Unsteady boundary layer flow over a permeable curved stretching/shrinking surface. *Eur. J. Mech.* **2015**, *51*, 61–67. [CrossRef]